The scramblases VMP1 and TMEM41b are required for primitive endoderm specification by targeting WNT signaling

Markus Holzner1, Tea Sonicki1, Hugo Hunn1, Vamshidhar R. Gade2, Karsten Weis2, Anton Wutz1#, and Giulio Di Minin1#

1 Institute of Molecular Health Sciences, Department of Biology, ETH Zurich, Zurich, Switzerland
2 Institute of Biochemistry, Department of Biology, ETH Zurich, Zurich, Switzerland

corresponding authors: awutz@ethaz.ch (AW); giulio.diminin@biol.ethz.ch (GDM)

Keywords: Vmp1, Tmem41b, WNT pathway, ESCs, Primitive endoderm, Autophagy and Lipid droplets

Characters (with space): 33500
Abstract: 158 words
4 figures

SUMMARY

The ER resident proteins VMP1 and TMEM41b share a DedA domain, which confers lipid scramblase activity. Loss of either gene results in embryonic lethality in mice and defects in autophagy and lipid droplet metabolism. To understand their role in pluripotency and specification, we generated Vmp1 and Tmem41b mutant mouse embryonic stem cells (ESCs). We observe that ESCs carrying mutations in Vmp1 and Tmem41b are viable, proliferate normally, and maintain a largely intact pluripotency-associated transcriptional profile. Despite clear defects in the accumulation of LC3-positive autophagosomes and lipid droplets, ESCs carrying combined mutations in Vmp1 and Tmem41b can differentiate into a wide range of embryonic cell types. However, the combined loss of Vmp1 and Tmem41b impairs the specification of primitive endoderm-like cells. We observe a delayed differentiation of mutant ESCs into extra-embryonic endoderm stem (XEN) cells. Mechanistically, we discover that mutant cells upregulate DDIT3, a WNT inhibitor. Chemical stimulation of the WNT cascade can rescue the differentiation delay. Our findings reveal a redundant function of the lipid scramblases VMP1 and TMEM41b and identify a specific role in signaling during extra-embryonic endoderm development.

INTRODUCTION

Vesicle trafficking and membrane synthesis are intricately interconnected within cellular signaling networks. Lipid scramblases, with their property to shape lipid membrane composition, play a crucial role in facilitating inter-organelle communication. Beyond their integral involvement in maintaining cell functionality, recent studies have unveiled their implications in various pathological conditions, such as viral infection, cancer development, and inflammatory diseases (Hama et al., 2022). The vacuole membrane protein 1 (VMP1) and transmembrane protein 41B (TMEM41B) are lipid scramblases with a highly conserved DedA domain (Ghanbarpour et al., 2021; Li et al., 2021). They localize at the ER membrane and are distinguished from other ER-associated flippases or scramblases by the property to facilitate bi-directional lipid diffusion in an ATP- and Ca2+-independent manner. VMP1 and TMEM41B are necessary for autophagosome formation (Molejon et al., 2013; Moretti et al., 2018), lipid droplet metabolism (Li et al., 2021; Morishita et al., 2019), and lipoprotein formation (Hama et al., 2022). Additional reports proposed a more global role in ER protein homeostasis (Tornero-Ecija et al., 2022) and vesicle transport (Bard et al., 2006). Despite multifaceted functions, their absence does not influence cell survival significantly. Compensatory mechanisms shared by VMP1 and TMEM41B or other ER scramblases likely maintain cellular homeostasis. While VMP1 depletion leads to a pronounced defect in autophagosome assembly (Molejon et al., 2013; Moretti et al., 2018), TMEM41B appears to play a pivotal role in sustaining lipid droplet homeostasis and serves as a crucial factor in RNA virus replication (Hoffmann et al., 2021; Huang et al., 2021). However, a systematic comparison between the activities of VMP1 and TMEM41B has not yet been performed.

VMP1 and TMEM41B are both essential during embryonic development. Vmp1 (Morishita et al., 2019) and Tmem41b (Van Alstyne et al., 2018) deficient mice die around E8.5 following severe developmental delay. Prior studies formulated a hypothesis where VMP1 restricts the transfer of vital nutrients to the embryo by blocking the synthesis and release of lipoproteins from the visceral endoderm. Nonetheless, mice with defects in lipoprotein biogenesis experience mortality at later stages (Farese et al., 1995; Raabe et al., 1998), specifically at E10.5. This observation implies a distinct and earlier involvement of VMP1 and TMEM41B in embryo development.

During implantation, the mouse embryo is composed of three lineages: the trophectoderm, which gives rise to the placenta; the primitive endoderm (PE), contributing to the yolk sac; and the epiblast (EPI), which is primed to develop into the embryo (Arnold and Robertson, 2009). The EPI and PE are specified within the inner cell mass (ICM) of the blastocyst. Defects in the formation of these lineages are challenging to characterize *in vivo* as they appear pre-implantation and due to the small embryo size. To investigate the role of Vmp1 and Tmem41b in early embryo lineage specification, we studied the ability of mutant cells to differentiate *in vitro* towards embryonic germ layers. We found that a combined Vmp1 and Tmem41b mutation in ESCs results in a specific defect in PE formation and a delayed conversion to extra-embryonic endoderm cells (XEN). This delay is caused by imbalanced WNT signaling and can be rescued through artificial WNT activation.

RESULTS

Vmp1 and Tmem41b mutant ESCs accumulate LC3+ autophagosomes and lipid droplets

To assess the influence of a Vmp1 or Tmem41b depletion on mouse ESCs and in early embryo development, we engineered genomic deletions using CRISPR/Cas9 targeted mutagenesis. Vmp1 was mutated by introducing a frameshift in exon 2 (Fig.1A). Loss of Vmp1 protein was confirmed in independent mutant ESC clones ($Vmp1^{KO}$) (Fig.S1A). To abrogate Tmem41b expression, we deleted the genomic region between exons 2 and 3 (Fig.1A), which encodes the first transmembrane domain of the protein ($Tmem41b^{KO}$). This mutation is predicted to compromise the protein topology. Additionally, the splicing of exon 1 to exon 4 produces a frameshift, suggesting a null allele. The deletion was confirmed on the genomic DNA (Fig.S1B). Tmem41b mRNA levels were strongly reduced (Fig.S1C-D).

Vmp1 and Tmem41b mutant ESCs showed similar morphology (Fig.1B), proliferation (Fig.S1E), and expression of pluripotency markers (Fig.S1F-G) compared to WT ESCs. We confirmed that the pluripotency network was unchanged by a transcriptomic analysis performed in individual Vmp1 and Tmem41b mutant cells. This analysis also showed that the transcription profile of cells was marginally affected, consistent with earlier results of ESC characterization (Fig.S1I-J and Table S2).

To test the effect of Vmp1 and Tmem41b mutations on autophagy, we measured the accumulation of LC3+ autophagosomes. We found an increase of LC3+ puncta in both mutants compared to WT ESCs (Fig.1C and Fig.S2A-B). Interestingly, the increased frequency of LC3+ puncta was similar in Vmp1 (4X) and Tmem41b (3,5X) mutant cells. Next, mutant cells were analyzed for the retention of lipid droplets (LD). To amplify LDs, we treated all samples with oleic acid (OA) and visualized LDs by BODIPY staining. We observed that Vmp1 and Tme41b mutations led to an increase of 4 times LD frequency with respect to WT cells. These results suggest that both Vmp1 and Tmem41b contribute to autophagosome and lipid droplet metabolism in ESCs, recapitulating earlier studies performed in other cellular systems (Li et al., 2021; Moretti et al., 2018). The direct comparison of mutation effects revealed a similar contribution of VMP1 and TMEM41B in both processes.

Vmp1 and Tmem41b activity is not required for ESC self-renewal

We generated double mutant cell lines to characterize potential redundant functions between VMP1 and TMEM41B. A Tmem41b mutation was engineered in Vmp1 mutant ESCs (Double KO) (Fig.S1A-D). Several independent mutant clones were obtained. Notably, Double KO cells showed a regular ESC morphology (Fig.S1H) and proliferation rate (Fig.S1E). The absence of Vmp1 and Tmem41b did not affect secretory compartments, as ER, Golgi apparatus, and Late Endosomes appeared normal in mutant cells (Fig.S3A). Double KO cells showed a limited perturbation in gene expression (Fig.1E). The combined mutations did not result in a greater number of differentially regulated genes compared to Vmp1^{KO} cells (Fig.S3C). Minimal overlap of differentially expressed genes was detected among Vmp1, Tmem41b and Double KO mutant cell lines (Fig.S3B-C). Additionally, we did not observe enrichment for genes that are involved in defined cellular processes (Fig.1F, Fig.S3D-E). The pluripotency network, as also shown by IF staining (Fig.S1F-G), was not perturbed in Double KO cells. We conclude that Vmp1 and Tmem41b are not essential for maintaining ESC pluripotency.

Vmp1 and Tmem41b have redundant functions

LC3 staining showed that Double KO cell lines present an exacerbated phenotype in autophagosome accumulation compared to single mutants. In the Double KO, we did not detect an additional increase in the number of autophagosomes per cell (Fig.1G

141 and Fig.S2A-B). However, 14% of LC3 clusters in the Double KO had a larger size
142 (>3µm), compared to the 8% of autophagosomes across the single mutations and 3%
143 in the WT condition (Fig.1H and Fig.S2C).
144 The simultaneous depletion of Vmp1 and Tmem41b had a greater impact on
145 LD formation. Double KO cells showed a drastic increase of LD number in the absence
146 of oleic acid treatment, whereas in WT and Vmp1 and Tmem41b mutant conditions,
147 LDs were clearly observed just after OA treatment (Fig.1I-J and Fig.S2D-E). As
148 BODIPY could also stain lipid-containing compartments like autophagosomes
149 (O'Rourke et al., 2009), we confirmed the enriched lipid droplets in Double KO cells
150 with refractive index tomography, a labelling-independent technique (Fig.1K and
151 Fig.S2F-G). Together, these results indicate that Vmp1 and Tmem41b share
152 redundant functions, as the combined mutation of both genes exacerbates
153 autophagosome and lipid droplet accumulation.
154
155 **Loss of Vmp1 and Tmem41b affects ESC potential to differentiate into primitive**
156 **endoderm**
157 To assess the effect of Vmp1 and Tmem41b on the differentiation potential of ESCs,
158 we used embryoid body (EB) differentiation (Fig.2A). After 6 days of differentiation,
159 EBs derived from WT ESCs showed increased expression of ectoderm (Sox1 and
160 Fgf5), mesoderm (Actc1 and Brachyury) and endoderm (Gata6 and Dab2) genes
161 (Fig.2B and Fig.S4A), while the expression of pluripotency markers (Nanog and
162 Pou5f1) was lost (Fig.2B and Fig.S4A). We evaluated variations in the differentiation
163 potential of mutant cells by comparing the expression of these markers by RT-qPCR.
164 For each mutant, the differentiation potential of two independent clones was tested.
165 Vmp1, Tmem41b, and double mutant ESCs formed well-defined EBs that resembled
166 those of WT cells. All cell lines efficiently differentiated into the ectoderm and
167 mesoderm lineages (Fig.2C and Fig.S4B-C). Notably, Double KO EBs showed a
168 decreased expression of the endoderm markers Dab2 (100%) and Gata6 (57% of
169 experiments) (Fig.2C and Fig.S4C). Neither single mutant showed a similar failure in
170 Dab2 expression, even if some variability was detected between the analyzed clones.
171 In the single mutants, we noticed a decreased endoderm specification, as shown by
172 Gata6 expression levels in experiments performed with Vmp1^{KO} (56% of experiments)
173 and Tmem41b^{KO} (58%) cells (Fig.2C and Fig.S4C). Our results indicate that combined

174 mutation of Vmp1 and Tmem41b leads to reduced Dab2 expression and predisposes
175 to variability in the expression of other endodermal genes.
176 We confirmed the differentiation potential of Double KO cells into ectodermal
177 lineages by generating SOX1-positive spinal cord organoids (Fig.S4D). Mesodermal
178 differentiation was inferred from the ability of double mutant EBs to form contractile
179 cardiomyocytes after plating (Video S1-2). We subsequently sectioned day 6 EBs to
180 evaluate protein expression and distribution of endoderm markers by IF. Expression
181 of GATA4, GATA6, and SOX17 was detected but noticeably decreased in Double KO
182 compared to WT EBs (Fig.2D-E). Decreased GATA4 and GATA6 staining was
183 pronounced in EB border regions, which resemble the primitive endoderm layer
184 (Zeevaert et al., 2020). In line with these findings, we confirmed the absence of DAB2
185 in Double KO EBs (Fig.2F). Dab2 is mainly expressed in the primitive endoderm, while
186 the other markers are known to be expressed in both primitive and definitive
187 endoderm.
188 The significant reduction in both mRNA and protein levels of Dab2, along with
189 the weakened expression of endoderm markers at the edges of embryoid bodies,
190 provides evidence that the absence of Vmp1 and Tmem41b compromises the
191 formation of primitive endoderm.
192
193 **Combined Vmp1 and Tmem41b mutations delay ESC differentiation into extra-**
194 **embryonic endoderm stem (XEN) cells**
195 We tested the ability of Double KO ESCs to differentiate into extra-embryonic
196 endoderm stem (XEN) cells to characterize endodermal differentiation further. XEN
197 cells are a useful model of PE cells, with which they share signaling programs, gene
198 expression, and differentiation potential (Kruithof-de Julio et al., 2011). Double KO and
199 WT cells were differentiated into XEN cells with Activin A and Retinoic Acid (Niakan et
200 al., 2013). After 6 days, WT ESCs efficiently differentiated into XEN clusters (Fig.3A),
201 exhibiting a stellate and refractile morphology (Niakan et al., 2013). In Double KO cells,
202 the formation of XEN clusters was substantially reduced. We characterized XEN
203 identity by analyzing the expression of XEN markers by RT-qPCR (Fig.S5A) and
204 immunostaining (Fig.3B and Fig.S5B). It is worth noting that the small number of
205 derived XEN cells from Double KO ESCs can be expanded for multiple passages, as
206 shown in Fig.S5C. This result suggests that the loss of Vmp1 and Tmem41b does not

entirely prevent XEN specification, but rather causes a delay in the differentiation process.

WNT signaling defect in Vmp1 and Tmem41b mutant cells impair XEN specification

To characterize the effect of Vmp1 and Tmem41b double mutation on XEN specification, we analyzed the transcriptomic profile of Double KO and WT cells during the differentiation process. On day two of differentiation, we detected the induction of XEN-associated genes (Ngondo et al., 2018) in WT cells. These genes, however, were only poorly expressed in Double KO cells (Fig.3C-D and Fig.5E). Intriguingly, we did not observe any further perturbation in the transcription of genes involved in lipid metabolism, autophagy, or ER maintenance (Fig.S5D).

Instead, Double KO cells show specific deregulation of genes related to the WNT pathway (Fig.3E-F). A close analysis of these genes allowed to identify several well-established WNT-target genes, including Frzb, Sox17, Wnt3, and Ccdnd1 (Du et al., 2009; Tetsu and McCormick, 1999; Zhang et al., 2009). Their down-regulation strongly suggested a decreased activity of the WNT pathway in Double KO cells and might explain the observed defect in XEN specification (Athanasouli et al., 2023). Interestingly, Ddit3 was strongly upregulated in Double KO cells. DDIT3 acts as an inhibitor of the WNT signaling by repressing the transcriptional activity of the TCF7/TCF4 complex (Chiu et al., 2019). We confirmed increased levels of the DDIT3 protein in Double KO cells (Fig.4A) and quantified a fourfold increase over WT cells (Fig.4B).

Finally, we attempted to rescue the defect in XEN differentiation of double mutant cells by chemically activating WNT signaling. We employed the GSK3β kinase inhibitor (CHIR), as a WNT agonist. GSK3β inhibition did not affect XEN specification in WT ESCs. However, WNT activation significantly enhanced XEN cell cluster formation in double mutant ESCs (Fig. 3D-F and Fig. S5B). Collectively, our data indicate how Vmp1 and Tmem41b affect WNT signaling and explain the delay in primitive endoderm specification.

241 **DISCUSSION**

242 Vmp1 and Tmem41b have been recently identified in genetic screens designed to
243 study various cellular processes, like autophagy, lipid metabolism, virus maturation,
244 pathway modulation, and ER stress. The pleiotropic function and peculiar structure of
245 the DedA domain have prompted multiple studies addressing its mode of action and
246 role in cellular homeostasis. An important point under evaluation is whether Vmp1 and
247 Tmem41b work cooperatively or show specialization for different cellular processes.
248 To address this question, we targeted Vmp1 and Tmem41b genes in ESCs and
249 introduced mutations abrogating their expression. This allowed us to directly compare
250 the specificity of Vmp1 and Tmem41b in multiple processes. We report that their
251 absence similarly affects autophagy and lipid droplet accumulation. Moreover, we
252 show that the simultaneous loss of both genes exacerbates defects of single mutants,
253 particularly in LD formation. Our findings unveil a partial redundancy between Vmp1
254 and Tmem41b activity. It will be interesting to understand if variating expression levels
255 of Vmp1 and Tmem41b can account for their redundancy or dominance in different
256 cellular systems. This is especially relevant since Vmp1 expression is known to be
257 influenced by cell signaling (Lo Re et al., 2012; Wang et al., 2020).

258 The embryonic lethality caused by Vmp1 and Tmem41b mutations (Morishita
259 et al., 2019; Van Alstyne et al., 2018) during development may be explained by the
260 defective primitive endoderm specification that we detected *in vitro*. Embryoid body
261 experiments and the direct differentiation of ESCs to extra-embryonic endoderm stem
262 (XEN) cells support a specific delay in PE formation in double mutant cells.
263 Interestingly, it has been reported that other mutations leading to PE delay cause
264 retardation and embryo lethality at E8.5 (Futterer et al., 2012), mirroring phenotypes
265 of Vmp1 or Tmem41b mutant embryos. While both scramblases are needed in mice
266 for regular development, the depletion of both genes is required to cause a
267 differentiation delay in ESCs. More permissive *in vitro* growth conditions may explain
268 the requirement for the depletion of both genes to manifest this phenotype in cell
269 culture. It is worth noting that single Vmp1^{KO} or Tmem41b^{KO} cells also showed subtle
270 defects in endoderm specification in embryoid bodies, albeit less consistently than
271 Double KO cells. (Fig.2C). The finding of WNT signaling deregulation in Vmp1 and
272 Tmem41b XEN cells explains the specification delay detected in mutant cells:
273 WNT/TCF7L1 transcriptional response is necessary *in vitro* and *in vivo* to promote PE
274 expansion (Athanasouli et al., 2023). Retardation – not impairment – of PE

specification induced by Vmp1 or Tmem41b mutations may permit embryo implantation but the accumulation of defects likely blocks development during gastrulation.

It is unlikely that issues in autophagy or lipid/lipoprotein metabolism alone cause embryo arrest. Both KO embryos die earlier than day E8.5 with severe developmental delay, which is already evident at E7.5. Mutant mice with autophagy or LD metabolism defects reach the pup stage (Kuma et al., 2017) or die at E10.5 after gastrulation and during organogenesis (Farese et al., 1995; Raabe et al., 1998), respectively. We propose that PE defects in Vmp1/Tmem41b depleted cells are caused by the increased expression of the WNT repressor DDIT3 which we show at the transcriptional and protein level in KO cells (Fig.4F). DDIT3 can be activated via the PERK/ATF4 pathway by ER stress (Rozpedek et al., 2016) or calcium-dependent mechanisms upon Vmp1 depletion in the absence of ER stress (Li et al., 2023). Notably, downstream activation of the WNT cascade fully rescues the defects of Vmp1 and Tmem41b double mutant cells during XEN specification.

This work presents novel evidence illustrating the roles of Vmp1 and Tmem41b in acting at the interface of cell homeostasis and signaling. Applying the generated cellular systems, future studies will help clarify redundant mechanisms shared by these scramblases. Furthermore, the role of Vmp1 and Tmem41b in modulating the WNT cascade may extend to other signaling networks, revealing other cross-connections between cellular pathways and metabolic processes.

MATERIALS AND METHODS

Cell Culture

Mouse ES cells were maintained as previously described in chemically defined 2i medium with added leukemia inhibitory factor (LIF) as described in Di Minin et al. (Di Minin et al., 2022). Base media composition: DMEM (Gibco, #41965039), 15% FBS (Biowest, #S1810-500) 1% sodium pyruvate (Gibco, 11360-070), 1% non-essential amino acids (Gibco, #11140-035). Lif (2000 U/mL, homemade), PD0325901 (1 μM, AxonMedchem, #391210-10-9) and Chiron (3 μM, AxonMedchem, #252917-06-9) are added fresh before use.

309 **EB differentiation**

310 To obtain embryonic bodies (EBs), 200k ESCs were plated on Day1 in ESCs base
311 media without 2i and LIF (see cell culture) into a well of a Sphericalplate5D
312 (Kugelmeiers). On Day4, EBs have formed and are transferred to a pHEMA coated
313 6cm culture dish and cultured until Day6. EBs are then collected and subjected to RNA
314 extraction and RT-qPCR analysis or prepared for sectioning and immunofluorescence.
315 In brief, EBs are fixed in 4% PFA for 30 min, cryoprotected in 10%, 20% and 30%
316 sucrose and then embedded and frozen in Tissue Freezing Medium (Leica,
317 #14020108926). 15 µm sections were prepared on a cryotome, mounted onto
318 Superfrost Plus Adhesion slides (VWR international GmBH, #631-0108) and
319 processed for immunofluorescence staining.

320

321 **Cardiomyocyte differentiation**

322 EBs were formed as previously described. On Day4, EBs were collected and seeded
323 onto a non-treated 10cm dish, maintaining ESC base media. Cardiomyocytes
324 randomly specified and were observed as early as on Day6 of differentiation.

325

326 **Spinal Cord Organoids (SCOs) formation**

327 For derivation of SCOs, ESCs were plated in EBs media (DMEM- F12 (Gibco) and
328 Neurobasal Medium (Gibco) (1:1 ratio) supplemented with 200 mM L-glutamine and
329 10% of Knockout serum replacement) on Sphericalplate 5D dishes (Kugelmeiers AG).
330 On day 2, SCOs were transferred in 10 cm tissue culture dishes and treated with RA
331 (10 nM). SCOs were collected and processed for analysis at day 5.

332

333 **Xen Differentiation**

334 XEN cells were obtained following a protocol by Niakan et al. with minor changes
335 (Niakan et al., 2013). In brief, 230k cells were plated in XEN medium on a gelatin-
336 coated 3cm dish. The next day, the media was replaced with Xen medium containing
337 0.1 µM retinoic acid (Thermo Fischer, #17110052) and 10 ng/mL Activin A (Peprotech,
338 #120-14). On Day4, the medium was again replaced by XEN medium, no further
339 supplements were added, and on Day6 samples were either analyzed by IF or qPCR.
340 Rescue of double KO Xen differentiation was performed by adding 1 µM Chiron
341 (AxonMedchem, #252917-06-9) at Day2, together with the retinoic acid and Activin A.
342 Media was changed on day 4 to Xen medium. XEN medium composition: RPMI 1640

343 (Gibco, #61870010), GlutaMAX^{TM} (Gibco, #61870036), 15% FBS (Biowest, #S1810-
344 500), 0,1 mM ß-mercaptoethanol (Sigma, #BCCB9882).
345
346 **CRISPR-Cas9 editing to generate mutant ESC lines**
347 Vmp1: the gRNA (gagacgcatagcaatgagta) was cloned into a px330 vector (Addgene,
348 #158973). Per 3cm well, 300k ESCs were plated and transfected with 2.5 µg of gRNA
349 containing plasmid, as well as 0.25 µg of a GFP expressing plasmid (pCMV-GFP).
350 GFP-positive cells were enriched by FACS and plated as single cells. Colonies were
351 picked. Analysis by WB was used to identify identified VMP1 KO lines. Tmem41b: the
352 gRNAs (gtatgtttgacctgggcgaa and gagtgacatgtggaaatcag) were cloned into px330
353 vectors, and KO clones were derived as described above. PCR analysis of the edited
354 locus (FW: atcttggacagggggagttc RV: gaccaggggttcattgtcatt and FW:
355 cagcacacacctttaatccagc RV: gccacatagcaagcttaagagc) identified KO clones. qPCR of
356 mRNA from Exon 2 (edited locus, N-terminal end) and Exon 7 (C-terminal end) further
357 confirmed the absence of mRNA.
358
359 **Proliferation assay**
360 100k ESCs were plated in a well of a MW12. 48h later, cells were collected and
361 counted. Proliferation rates were calculated as relative factor of cells collected over
362 cells seeded.
363
364 **LC3 staining and size characterization**
365 100k cells were plated on cover-slips, pre-treated with Matrigel (Corning, # 354277),
366 in N2B27 media. N2B27 composition: 50 mL Neurobasal media (Gibco, # 2348949),
367 50 mL Advanced DMEM F12 (Gibco, # 12634010), 4% BSA (Gibco, # 15260), 1% L-
368 Glutamine (Gibco, # 25030024), 1% B27 supplement (Gibco, # 2336837), 0,5% N2
369 supplement (Gibco, # 2328253), and 0,1 mM ß-mercapotethanol (Sigma,
370 #BCCB9882). The next day, samples were fixed in 4% PFA for 15 min, washed 3 times
371 with PBS and then treated with ice-cold MeOH for 5 min on RT. The staining was then
372 performed as described below. Quantification was performed with the Fiji plugin
373 TrackMate (Ershov et al., 2022; Tinevez et al., 2017) to automatically detect puncti
374 with a diameter of 1, 2, and 3 microns at a threshold of 600, 200 and 150, respectively.
375 Nuclei were detected at an average size of 15 microns with a threshold of 10. Unique

376 particles were annotated for 5 different frames for each condition and shown as
377 particles per cell. The experiment was repeated 3 times.
378
379 **LD staining and RF microscopy**
380 Samples were plated as for the LC3 staining. For samples treated with oleic acid,
381 200 µM (Sigma-Aldrich, # O1008-1G) were added at plating, over-night. The next day,
382 samples were incubated in 5 µM BODIPY 493/503 (Invitrogen, #D3922) in PBS and
383 subsequently washed 3 times with PBS and fixed in 4 % PFA for 15 min. Samples
384 were then washed, stained with Dapi for 15 min at RT and mounted with Mowiol.
385 Quantification was performed using the Fiji plugin TrackMate (Ershov et al., 2022;
386 Tinevez et al., 2017) detecting droplets of 1, 2, and 3 microns in diameter at a threshold
387 of 900. Nuclei were detected at 10 micron and a threshold of 1.
388 For RF microscopy, 250k cells were plated per well of a 6 well glass bottom plate
389 (Cellvis, # P06-1.5H-N) in N2B27 media. After 36 h samples were treated with 200 µM
390 oleic acid o/n and then with BODIPY for 3 h. Samples were washed 3 times with PBS
391 and maintained in N2B27 for RF microscopy. The imaging was performed on
392 Tomocube HT-X1 instrument at 37C and 5 % CO2. At least 5-8 images were acquired
393 for each condition for each well. The z-stacks were acquired with 1.06 µm slices. Max
394 Intensity projections (MIP) are generated on the Tomostudio 3.3.9. The fluorescence
395 max intensity projections were resized to Refractive index tomograms for comparison.
396 The ROIs from each image were isolated for further analysis. Comdet plugin was used
397 for identifying high refractive index regions. The approximate particle size was 2 pixels
398 and Intensity threshold values were chosen individually for each image to avoid any
399 false positives or negatives.
400
401 **Immunofluorescence**
402 Samples were washed 3 times with PBS, fixed in 4% PFA for 10 min and again washed
403 3 times with PBS. Samples stained for LC3 were then treated for 5 min with 100%
404 MeOH at RT and washed again 3 times with PBS. Samples were then blocked and
405 permeabilized with 10% donkey serum (Jackson Immunoresearch, #017-000-121)
406 and 0,1% Triton X (Thermo Fischer, # HFH10) in PBS for 20 min and incubated with
407 primary antibodies at 4 °C over-night. Oct4 (1:100, Satna Cruz, # sc-5279), Nanog
408 (1:100, Abcam, # ab80892), Sox2 (1:50, R&D Systems #AF2018), Lc3 (1:200, Cell
409 Signalling, # 2775S), Pdi (1:200, Cell Signalling, # 3501S), Rcas1 (1:200, Cell

410 Signalling, # 12290S), Rab7 (1:200, Cell Signaling, # 9367S) Sox1 (1:50, R&D
411 Systems, # AF3369), Sox17 (1:200 R&D Systems, # AF1924-SP), Gata4 (1:100 R&D
412 Systems, # AF1700-SP), Gata6 (1:100 R&D Systems, # AF1700-SP), Dab2 (1:100
413 BD, # 610464). The next day, samples were washed 3 times with 0.1% Triton X in PBS
414 and then incubated with secondary antibodies and Dapi.
415
416 **Western Blot Analysis**
417 Cells were lysed in membrane buffer (150 mM NaCl, 50 mM Tris-HCl pH 7,5, 1 mM 2-
418 mercaptoethanol (Sigma, #M3148) and 1% CHAPS (Sigma, #C3023) in water).
419 Lysates were run on SDS-Page and transferred to nitrocellulose membranes. Bands
420 were detected with the Amersham ECL Prime Western Blotting Detection Reagents
421 (#RPN2232) and captured on Fujifilm Super RX-N films (#47410). Antibodies for Vmp1
422 (Cell Signalling, #12929S) were used at 1:1000 and DDIT3 1:1000 (Cell Signalling,
423 #2895T). Quantification of western blot bands was performed with ImageJ, normalized
424 to HSP90 (Santa Cruz, #sc-101494).
425
426 **RNA extraction and RT qPCR**
427 RNA was extracted with the RNeasy Kit (Quiagen, #74104) following the
428 manufacturer's instructions, including the on-column DNA digestion. EB and SCO
429 samples were pre-treated with the QIAshredder (Quiagen, #79656). cDNAs were
430 prepared using the Bio-Rad iScript Reverse Transcription Supermix for RT-qPCR
431 (#1708841). RT qPCR samples were prepared using the KAPPA SYBR R fast (Roche,
432 KK4611). Primer Sequences:
433 Tmem41b Exon2 FW: TGCAGAAGCTGGATCAGCAA, RV:
434 GAGCCTTGGCGTCATCCATA
435 Tmem41b Exon7 FW: GCAGGTAGAGCGTCACAGAG, RV:
436 TGCAGAGTTGTTCCTGCCTT
437 Sdha FW: CGTTATGTGAGGGGTGTGCCTT, RV:
438 CCTTACCAAACCTTGTGTCTGGA
439 Sox1 FW: ACGTAGCCAACGTAGACAC, RV: ATGAGCGTCGTCCCGTGG
440 Fgf5 FW: GCCTGTCCTTGCTCTTCCTCAT, RV: GGAGAAGCTGCGACTGGTGA
441 Actc1 FW: TGTAGGACCGTGTCGAAACC, RV: CGAAACCACACACTGTTACCG
442 Brachyury FW: TCTCTGGTCTGTGAGCAATGGT, RV:
443 TGCGTCAGTGGTGTGTAATGTG

Gata6 FW: GAAGCGCGTGCCTTCATC, RV: GTAGTGGTTGTGGTGTGACAGTTG
Dab2 FW: TTGATGATGTGCCTGATGCT, RV: TTTGCTTGTGTTGTCCCTGA
Sox17 FW: CCCAACACTCCTCCCAAAGTATC, RV:
TTCCCTGTCTTGGTTGATTTCT

Quantification and statistical analysis

Statistical analysis was performed using Python and GraphPad Prism. Data are presented as mean-centered and the standard deviation. All experiments were repeated with at least 3 independent biological replicates, unless stated otherwise. The statistical test used to evaluate significance is the Welch's *t* test. Statistical significance in the figures is denoted as follows: ns: $p > 0.05$, *: $p < 0.05$, **: $p < 0.01$, ***: $p < 0.001$.

RNA seq

RNA samples were submitted to the Functional Genomics Center in Zurich (FGCZ) for RNA sequencing. The quality of the RNA was determined with a Fragment Analyzer standard sensitivity RNA measurement (SS RNA kit (15 nt), Agilent, Waldbronn, Germany). The measured concentrations (> 50 ng/µl) and RIN (>9.9) values qualified for a Poly-A enrichment strategy in order to generate the sequencing libraries applying the TruSeq mRNA Stranded Library Prep Kit (Illumina, Inc, California, USA). After Poly-A selection using Oligo-dT beads the mRNA was reverse-transcribed into cDNA. The cDNA was fragmented, end-repaired and polyadenylated before ligation of TruSeq UD Indices (IDT, Coralville, Iowa, USA). The quality and quantity of the amplified sequencing libraries were validated using a Fragment Analyzer SS NGS Fragment Kit (1–6000 bp) (Agilent, Waldbronn, Germany). The equimolar pool of samples was spiked into a NovaSeq6000 run targeting 20M reads per sample on a S1 FlowCell (Novaseq S1 Reagent Kit, 100 cycles, Illumina, Inc, California, USA). Reads from RNA-seq were first preprocessed by Trimmomatic (v0.40) (Bolger et al., 2014) to remove low-quality bases and adapters. Then, reads were aligned to mouse genome GRCm38 (release 81 version from Ensembl) using HISAT2 (v2.2.1) (Kim et al., 2019). HTSeq Count (v2.0.2) (Putri et al., 2022) was used to count reads for each gene (Ensembl GRCm38.81), ignoring reads on overlapped regions. Differentially expressed genes were defined by DESeq2 (v1.40.2) (Love et al., 2014). MA plot was generated using custom-made scripts. Genes significantly enriched show a fold

change > 1 and FDR (adjusted p-value) < 0.01. The read counts were transformed in RPKM for the heatmap representations of specific genes and pathways. The genes corresponding to germ-layer differentiation markers (including those for embryonic and extra-embryonic endoderm), biological processes, and signaling pathways were obtained through literature mining and the KEGG database (Table S1). The processed data are available as excel files (Table S2 and Table S3) and raw data have been deposited on NCBI SRA database under the accession: PRJNA1031567

Competing interest

The authors declare no competing interests.

Acknowledgments

We acknowledge the Functional Genomics Center Zurich (FGCZ) for technical support and Sungsik Lee from ScopeM facility for help on the RF microscopy. We thank G.J. Pereira, C. Fimiani, and U. Sutter for their help with reagents. We thank C. Ciaudo, A. Grison, J. Corn, and K. Basler for their helpful discussions. GDM was supported by the ETH Zurich Postdoctoral Fellowship Program as well as the Marie Curie Actions for People COFUND Program. This work was supported by grants from the Swiss National Science Foundation (SNF grants 31003A_152814/1 and 31003A_175643/1).

Author Contributions

Conceptualization: MH, AW and GDM; Data curation: MH, VG and GDM; Formal analysis: MH, TS, HH, VG, and GDM; Funding acquisition: KW, AW and GDM; Investigation: MH, AW and GDM; Methodology: MH, TS, HH, VG, and GDM; Project administration: AW, GDM; Resources: MH, KW, AW and GDM; Supervision: KW, AW and GDM; Validation: MH, GDM; Visualization: MH, VG and GDM; Writing – original draft: MH, AW and GDM; Writing – review & editing: MH, TS, HH, VG, KW, AW and GDM.

REFERENCES

Arnold, S.J., and Robertson, E.J. (2009). Making a commitment: cell lineage allocation and axis patterning in the early mouse embryo. Nat Rev Mol Cell Biol *10*, 91-103.

Athanasouli, P., Balli, M., De Jaime-Soguero, A., Boel, A., Papanikolaou, S., van der Veer, B.K., Janiszewski, A., Vanhessche, T., Francis, A., El Laithy, Y.*, et al.* (2023). The Wnt/TCF7L1 transcriptional repressor axis drives primitive endoderm formation by antagonizing naive and formative pluripotency. Nat Commun *14*, 1210.

Bard, F., Casano, L., Mallabiabarrena, A., Wallace, E., Saito, K., Kitayama, H., Guizzunti, G., Hu, Y., Wendler, F., Dasgupta, R.*, et al.* (2006). Functional genomics reveals genes involved in protein secretion and Golgi organization. Nature *439*, 604-607.

Bolger, A.M., Lohse, M., and Usadel, B. (2014). Trimmomatic: a flexible trimmer for Illumina sequence data. Bioinformatics *30*, 2114-2120.

Chiu, C.S., Tsai, C.H., Hsieh, M.S., Tsai, S.C., Jan, Y.J., Lin, W.Y., Lai, D.W., Wu, S.M., Hsing, H.Y., Arbiser, J.L.*, et al.* (2019). Exploiting Honokiol-induced ER stress CHOP activation inhibits the growth and metastasis of melanoma by suppressing the MITF and beta-catenin pathways. Cancer Lett *442*, 113-125.

Di Minin, G., Holzner, M., Grison, A., Dumeau, C.E., Chan, W., Monfort, A., Jerome-Majewska, L.A., Roelink, H., and Wutz, A. (2022). TMED2 binding restricts SMO to the ER and Golgi compartments. PLoS Biol *20*, e3001596.

Du, Y.C., Oshima, H., Oguma, K., Kitamura, T., Itadani, H., Fujimura, T., Piao, Y.S., Yoshimoto, T., Minamoto, T., Kotani, H.*, et al.* (2009). Induction and down-regulation of Sox17 and its possible roles during the course of gastrointestinal tumorigenesis. Gastroenterology *137*, 1346-1357.

Ershov, D., Phan, M.S., Pylvanainen, J.W., Rigaud, S.U., Le Blanc, L., Charles-Orszag, A., Conway, J.R.W., Laine, R.F., Roy, N.H., Bonazzi, D.*, et al.* (2022). TrackMate 7: integrating state-of-the-art segmentation algorithms into tracking pipelines. Nat Methods *19*, 829-832.

Farese, R.V., Jr., Ruland, S.L., Flynn, L.M., Stokowski, R.P., and Young, S.G. (1995). Knockout of the mouse apolipoprotein B gene results in embryonic lethality in homozygotes and protection against diet-induced hypercholesterolemia in heterozygotes. Proc Natl Acad Sci U S A *92*, 1774-1778.

Futterer, A., Raya, A., Llorente, M., Izpisua-Belmonte, J.C., de la Pompa, J.L., Klatt, P., and Martinez, A.C. (2012). Ablation of Dido3 compromises lineage commitment of stem cells in vitro and during early embryonic development. Cell Death Differ *19*, 132-143.

Ghanbarpour, A., Valverde, D.P., Melia, T.J., and Reinisch, K.M. (2021). A model for a partnership of lipid transfer proteins and scramblases in membrane expansion and organelle biogenesis. Proc Natl Acad Sci U S A *118*.

Hama, Y., Morishita, H., and Mizushima, N. (2022). Regulation of ER-derived membrane dynamics by the DedA domain-containing proteins VMP1 and TMEM41B. EMBO Rep *23*, e53894.

Hoffmann, H.H., Schneider, W.M., Rozen-Gagnon, K., Miles, L.A., Schuster, F., Razooky, B., Jacobson, E., Wu, X., Yi, S., Rudin, C.M.*, et al.* (2021). TMEM41B Is a Pan-flavivirus Host Factor. Cell *184*, 133-148 e120.

Huang, D., Xu, B., Liu, L., Wu, L., Zhu, Y., Ghanbarpour, A., Wang, Y., Chen, F.J., Lyu, J., Hu, Y.*, et al.* (2021). TMEM41B acts as an ER scramblase required for lipoprotein biogenesis and lipid homeostasis. Cell Metab *33*, 1655-1670 e1658.

Kim, D., Paggi, J.M., Park, C., Bennett, C., and Salzberg, S.L. (2019). Graph-based genome alignment and genotyping with HISAT2 and HISAT-genotype. Nat Biotechnol *37*, 907-915.

558 Kruithof-de Julio, M., Alvarez, M.J., Galli, A., Chu, J., Price, S.M., Califano, A., and Shen, M.M.
559 (2011). Regulation of extra-embryonic endoderm stem cell differentiation by Nodal and Cripto
560 signaling. Development *138*, 3885-3895.
561 Kuma, A., Komatsu, M., and Mizushima, N. (2017). Autophagy-monitoring and autophagy-
562 deficient mice. Autophagy *13*, 1619-1628.
563 Li, T., Zhao, H., Guo, G., Xia, S., and Wang, L. (2023). VMP1 affects endoplasmic reticulum stress
564 sensitivity via differential modulation of the three unfolded protein response arms. Cell Rep
565 *42*, 112209.
566 Li, Y.E., Wang, Y., Du, X., Zhang, T., Mak, H.Y., Hancock, S.E., McEwen, H., Pandzic, E., Whan,
567 R.M., Aw, Y.C.*, et al.* (2021). TMEM41B and VMP1 are scramblases and regulate the
568 distribution of cholesterol and phosphatidylserine. J Cell Biol *220*.
569 Lo Re, A.E., Fernandez-Barrena, M.G., Almada, L.L., Mills, L.D., Elsawa, S.F., Lund, G., Ropolo,
570 A., Molejon, M.I., Vaccaro, M.I., and Fernandez-Zapico, M.E. (2012). Novel AKT1-GLI3-VMP1
571 pathway mediates KRAS oncogene-induced autophagy in cancer cells. J Biol Chem *287*, 25325-
572 25334.
573 Love, M.I., Huber, W., and Anders, S. (2014). Moderated estimation of fold change and
574 dispersion for RNA-seq data with DESeq2. Genome Biol *15*, 550.
575 Molejon, M.I., Ropolo, A., Re, A.L., Boggio, V., and Vaccaro, M.I. (2013). The VMP1-Beclin 1
576 interaction regulates autophagy induction. Sci Rep *3*, 1055.
577 Moretti, F., Bergman, P., Dodgson, S., Marcellin, D., Claerr, I., Goodwin, J.M., DeJesus, R., Kang,
578 Z., Antczak, C., Begue, D.*, et al.* (2018). TMEM41B is a novel regulator of autophagy and lipid
579 mobilization. EMBO Rep *19*.
580 Morishita, H., Zhao, Y.G., Tamura, N., Nishimura, T., Kanda, Y., Sakamaki, Y., Okazaki, M., Li, D.,
581 and Mizushima, N. (2019). A critical role of VMP1 in lipoprotein secretion. Elife *8*.
582 Ngondo, R.P., Cirera-Salinas, D., Yu, J., Wischnewski, H., Bodak, M., Vandormael-Pournin, S.,
583 Geiselmann, A., Wettstein, R., Luitz, J., Cohen-Tannoudji, M.*, et al.* (2018). Argonaute 2 Is
584 Required for Extra-embryonic Endoderm Differentiation of Mouse Embryonic Stem Cells. Stem
585 Cell Reports *10*, 461-476.
586 Niakan, K.K., Schrode, N., Cho, L.T., and Hadjantonakis, A.K. (2013). Derivation of
587 extraembryonic endoderm stem (XEN) cells from mouse embryos and embryonic stem cells.
588 Nat Protoc *8*, 1028-1041.
589 O'Rourke, E.J., Soukas, A.A., Carr, C.E., and Ruvkun, G. (2009). C. elegans major fats are stored
590 in vesicles distinct from lysosome-related organelles. Cell Metab *10*, 430-435.
591 Putri, G.H., Anders, S., Pyl, P.T., Pimanda, J.E., and Zanini, F. (2022). Analysing high-throughput
592 sequencing data in Python with HTSeq 2.0. Bioinformatics *38*, 2943-2945.
593 Raabe, M., Flynn, L.M., Zlot, C.H., Wong, J.S., Veniant, M.M., Hamilton, R.L., and Young, S.G.
594 (1998). Knockout of the abetalipoproteinemia gene in mice: reduced lipoprotein secretion in
595 heterozygotes and embryonic lethality in homozygotes. Proc Natl Acad Sci U S A *95*, 8686-
596 8691.
597 Rozpedek, W., Pytel, D., Mucha, B., Leszczynska, H., Diehl, J.A., and Majsterek, I. (2016). The
598 Role of the PERK/eIF2alpha/ATF4/CHOP Signaling Pathway in Tumor Progression During
599 Endoplasmic Reticulum Stress. Curr Mol Med *16*, 533-544.
600 Tetsu, O., and McCormick, F. (1999). Beta-catenin regulates expression of cyclin D1 in colon
601 carcinoma cells. Nature *398*, 422-426.
602 Tinevez, J.Y., Perry, N., Schindelin, J., Hoopes, G.M., Reynolds, G.D., Laplantine, E., Bednarek,
603 S.Y., Shorte, S.L., and Eliceiri, K.W. (2017). TrackMate: An open and extensible platform for
604 single-particle tracking. Methods *115*, 80-90.

605 Tornero-Ecija, A., Tabara, L.C., Bueno-Arribas, M., Anton-Esteban, L., Navarro-Gomez, C.,
606 Sanchez, I., Vincent, O., and Escalante, R. (2022). A Dictyostelium model for BPAN disease
607 reveals a functional relationship between the WDR45/WIPI4 homolog Wdr45l and Vmp1 in
608 the regulation of autophagy-associated PtdIns3P and ER stress. Autophagy *18*, 661-677.
609 Van Alstyne, M., Lotti, F., Dal Mas, A., Area-Gomez, E., and Pellizzoni, L. (2018).
610 Stasimon/Tmem41b localizes to mitochondria-associated ER membranes and is essential for
611 mouse embryonic development. Biochem Biophys Res Commun *506*, 463-470.
612 Wang, C., Peng, R., Zeng, M., Zhang, Z., Liu, S., Jiang, D., Lu, Y., and Zou, F. (2020). An
613 autoregulatory feedback loop of miR-21/VMP1 is responsible for the abnormal expression of
614 miR-21 in colorectal cancer cells. Cell Death Dis *11*, 1067.
615 Zeevaert, K., Elsafi Mabrouk, M.H., Wagner, W., and Goetzke, R. (2020). Cell Mechanics in
616 Embryoid Bodies. Cells *9*.
617 Zhang, Z., Deb, A., Zhang, Z., Pachori, A., He, W., Guo, J., Pratt, R., and Dzau, V.J. (2009).
618 Secreted frizzled related protein 2 protects cells from apoptosis by blocking the effect of
619 canonical Wnt3a. J Mol Cell Cardiol *46*, 370-377.
620
621

622 **FIGURE LEGENDS**

623

624 **Figure 1. Vmp1 and Tmem41b double KO ESCs display increased**
625 **autophagosome and lipid droplet accumulation**

626

627 **(A)** Schematic representation of the CRISPR/Cas9-mediated KO strategy for Vmp1
628 and Tmem41b genes. For depleting Vmp1 (top) a single gRNA inducing an indel
629 mutation has been used. In the case of the Tmem41b gene (bottom), two gRNAs were
630 used to delete exons 2 and 3. The sequences coding for transmembrane domains
631 (TM) are indicated in blue, the conserved DedA domain is highlighted in yellow, red
632 lines indicate cut sites of gRNAs. **(B)** Colony morphology of $VMP1^{KO}$ and $Tmem41^{KO}$
633 ESCs remains unchanged compared to WT ESCs. Scale bar: 100 µm. **(C)** VMP1 and
634 Tmem41b depletion induce accumulation of autophagosomes in ESCs. The graph
635 shows the quantification of LC3 puncta per cell of a representative experiment (see
636 Fig.S2A). Data were collected from more than 200 cells. For each KO condition, two
637 independent clones have been analyzed. Dots correspond to the frames analyzed per
638 sample. Data are represented as mean ± SD. The P-value is relative to the WT sample.
639 **(D)** Vmp1 and Tmem41b depletion leads to the accumulation of lipid droplets (LD) in
640 ESCs. Graph quantifies LD per cell in WT and KO ESCs (see Fig.S2D). ± oleic acid
641 treatment. At least 500 cells were analyzed for every condition; dots represent
642 independent biological replicates. Data are represented as mean ± SD. (**E-G)**
643 Transcriptional analysis of Double KO ESCs did not identify many deregulated genes.
644 **(E)** Shown are differentially regulated genes in Double KO ESCS in blue as MA plot.
645 Genes highlighted in red are pluripotency markers. **(F)** Differentially regulated genes
646 do not cluster in essential processes. The graph shows differentially expressed genes
647 of single and double KO ESCs by cellular processes. Dot size correlates to the number
648 of deregulated genes within a cellular process. **(G-H)** Double KO ESCs accumulate
649 LC3+ autophagosomes of increased size. **(G)** Shown are representative IF images of
650 WT and double KO ESCs stained for LC3. Nuclei are stained with Dapi. Scale bar:
651 20 µm. **(H)** Plotted is the quantification of LC3 puncta of 3 µm in diameter. For each
652 condition, two independent clones have been analyzed. Dots correspond to the frames
653 analyzed per sample. Data were collected from more than 200 cells. Data are
654 represented as mean ± SD. The P-value is relative to the Double KO sample with the
655 highest SD. **(I-J)** Double KO ESCs accumulate LDs without oleic acid treatment. **(I)**

656 Live cell staining of WT, Vmp1, Tmem41b, and double KO ESCs with BODIPY. Scale
657 bar: 20 µm **(J)** The number of LDs per cell is plotted for all KO clones. Data are
658 represented as mean ± SD. **(K)** Double KO ESCs present an increased amount of LD
659 visualized through refractive index microscopy (top) and co-stained with BODIPY.
660
661 **Figure 2. Double KO ESCs specify all germ layers, but not the primitive**
662 **endoderm**
663
664 **(A)** Schematic representation of an Embryonic Body (EB) which consists of 3 different
665 lineages. The ectoderm expresses Fgf5 and Sox1 (grey), the mesoderm Actc1 and
666 Brachyury (blue), and the endoderm by Gata6. The surrounding region of the EB
667 corresponds to the primitive endoderm (green) and is marked by Gata6 and Dab2
668 expression. **(B)** ESCs differentiated to EBs express lineage markers for ectoderm
669 (Fgf5), mesoderm (Brachyury), endoderm (Gata6), and primitive endoderm (Dab2).
670 Graphs show mRNA levels of WT EBs normalized to the Sdha gene. Dots represent
671 biological independent experiments. Data are represented as mean ± SD. **(C)** Double
672 KO ESCs specifically show defects in expressing the primitive endoderm marker,
673 Dab2. qPCR analysis for Sox1, Actc1, and Dab2 mRNA expression in mutant EBs
674 relative to WT EBs. Two independent clones were analyzed per cell line. Each dot
675 represents an independent experiment. Data are represented as mean ± SD**.** The line
676 at 0,7 indicates an arbitrary threshold after which successful expression of the marker
677 is considered. **(D-F)** Double mutant EBs show decreased expression of endoderm
678 markers. Immunofluorescence images of EB sections stained for the endoderm
679 markers GATA4 and SOX17 **(D)**, GATA6 **(E)**, DAB2 **(F)**. WT in the top panel, two
680 independent clones for Double KO condition in the center and bottom panels. Nuclei
681 are stained with Dapi. Scale bar: 50 µm.
682
683 **Figure 3. XEN differentiation in Double KO cells is delayed**
684
685 **(A-B)** Double KO ESCs show a delay in XEN differentiation. **(A)** Brightfield images of
686 XEN cells at day 6 of differentiation in WT and Double KO cells. XEN islands are circled
687 in white in the Double KO condition. Scale bar: 100 µm. **(B)** Immunofluorescence
688 images of day 6 XEN cells stained for SOX17 and GATA4. Nuclei are stained with
689 Dapi, Scale bar: 150 µm. **(C-F)** Transcriptional analysis of XEN cells. **(C)** Differentially

690 expressed genes between Double KO and WT cells at day 2 during XEN specification.
691 XEN markers are labeled in red; differentially expressed genes in blue. **(D-E)** GO-Term
692 analysis of differentially expressed genes between Double KO and WT conditions in
693 ESCs and XEN cells in the context of developmental processes **(D)** and signaling
694 pathways **(E)**. Dot size corresponds to the number of differentially regulated genes.
695 **(F)** WNT pathway-related genes differentially expressed in Double KO cells. Heatmap
696 shows min to max expression of three biological replicates for WT and Double KO
697 XEN cells.
698
699
700 **Figure 4. Activation of WNT signaling fully rescues the delay of Double KO cells**
701 **in XEN differentiation**
702
703 **(A-B)** VMP1 and Tmem41b depletion promotes the increase of DDIT3 protein levels.
704 **(A)** Western Blot analysis of DDIT3 expression in WT and Double KO cells
705 differentiated to XEN cells for 2 days. HSP90 is shown as loading control. **(B)**
706 Quantification of increased DDIT3 protein levels in three biological replicates.
707 Expression relative to WT XEN cell and normalized to respective HSP90 expression.
708 Data are represented as mean ± SD. **(C-E)** Chiron-dependent WNT activation rescues
709 the delay of Double KO XEN differentiation. **(C)** Brightfield images show XEN clusters
710 of Double KO XEN cells (highlighted by white lines) with and w/o Chiron treatment.
711 Scale bar: 100 µm. IF staining for SOX17 and GATA4 **(D)** or DAB2 and GATA6 **(E)**;
712 nuclei are stained with Dapi. Scale Bar: 150 µm. **(F)** Schematic overview highlighting
713 the correlation between loss of Vmp1 and Tmem41b and decreased WNT signaling
714 via DDIT3.

Figure1

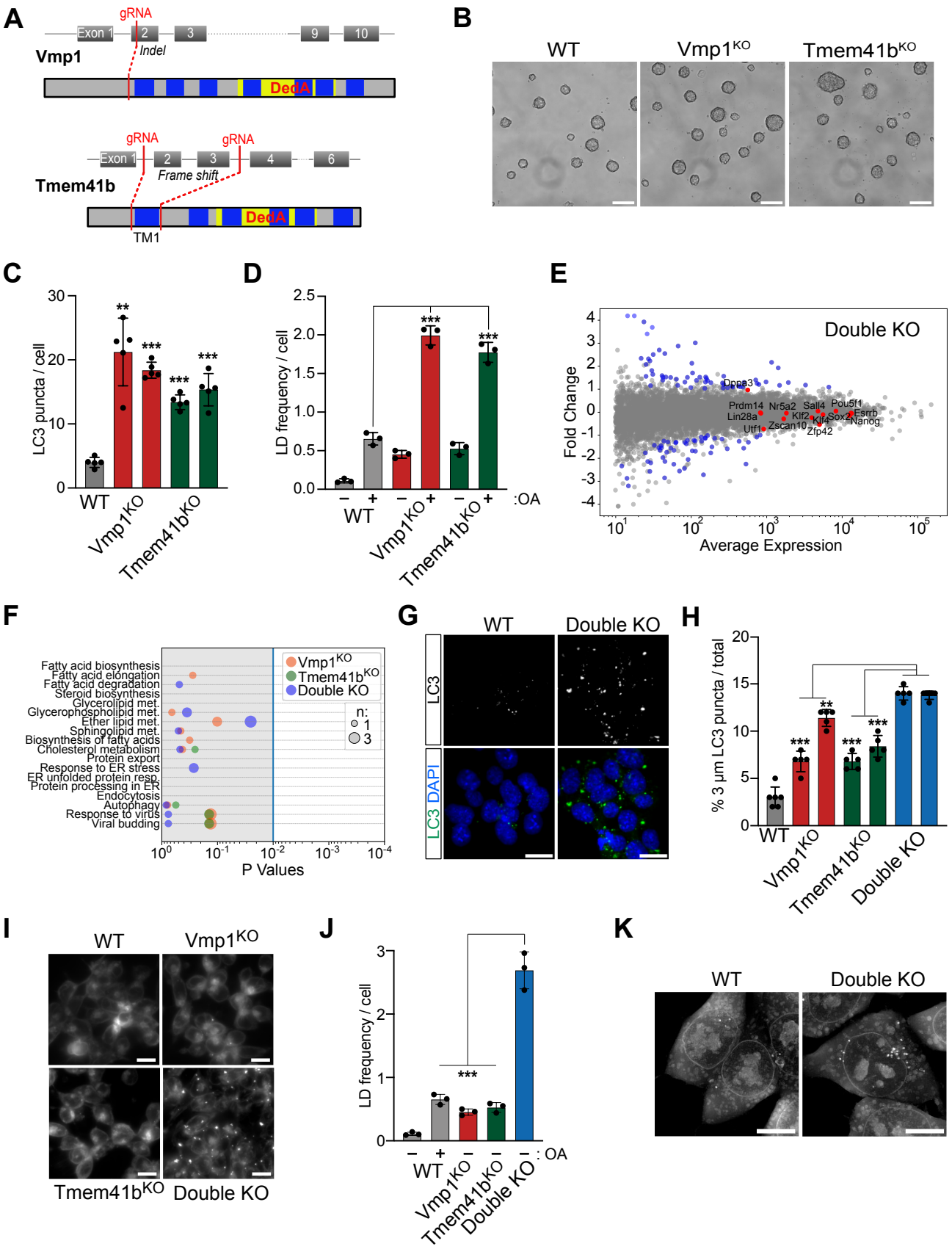
A
gRNA
Exon 1
2
3
9
10
Indel
Vmp1
DedA
gRNA
gRNA
Exon 1
2
3
4
6
Frame shift
Tmem41b
DedA
TM1
B
WT
Vmp1KO
Tmem41bKO
C
LC3 puncta / cell
WT
Vmp1KO
Tmem41bKO
D
LD frequency / cell
:OA
WT
Vmp1KO
Tmem41bKO
E
Double KO
Fold Change
Average Expression
Dppa3
Prdm14
Nr5a2
Sall4
Pou5f1
Lin28a
Klf2
Esrrb
Sox2
Klf4
Nanog
Utf1
Zscan10
Zfp42
F
Fatty acid biosynthesis
Fatty acid elongation
Fatty acid degradation
Steroid biosynthesis
Glycerolipid met.
Glycerophospholipid met.
Ether lipid met.
Sphingolipid met.
Biosynthesis of fatty acids
Cholesterol metabolism
Protein export
Response to ER stress
ER unfolded protein resp.
Protein processing in ER
Endocytosis
Autophagy
Response to virus
Viral budding
Vmp1KO
Tmem41bKO
Double KO
n:
1
3
P Values
G
WT
Double KO
LC3
LC3 DAPI
H
% 3 µm LC3 puncta / total
WT
Vmp1KO
Tmem41bKO
Double KO
I
WT
Vmp1KO
Tmem41bKO
Double KO
J
LD frequency / cell
: OA
WT
Vmp1KO
Tmem41bKO
Double KO
K
WT
Double KO

Figure 2

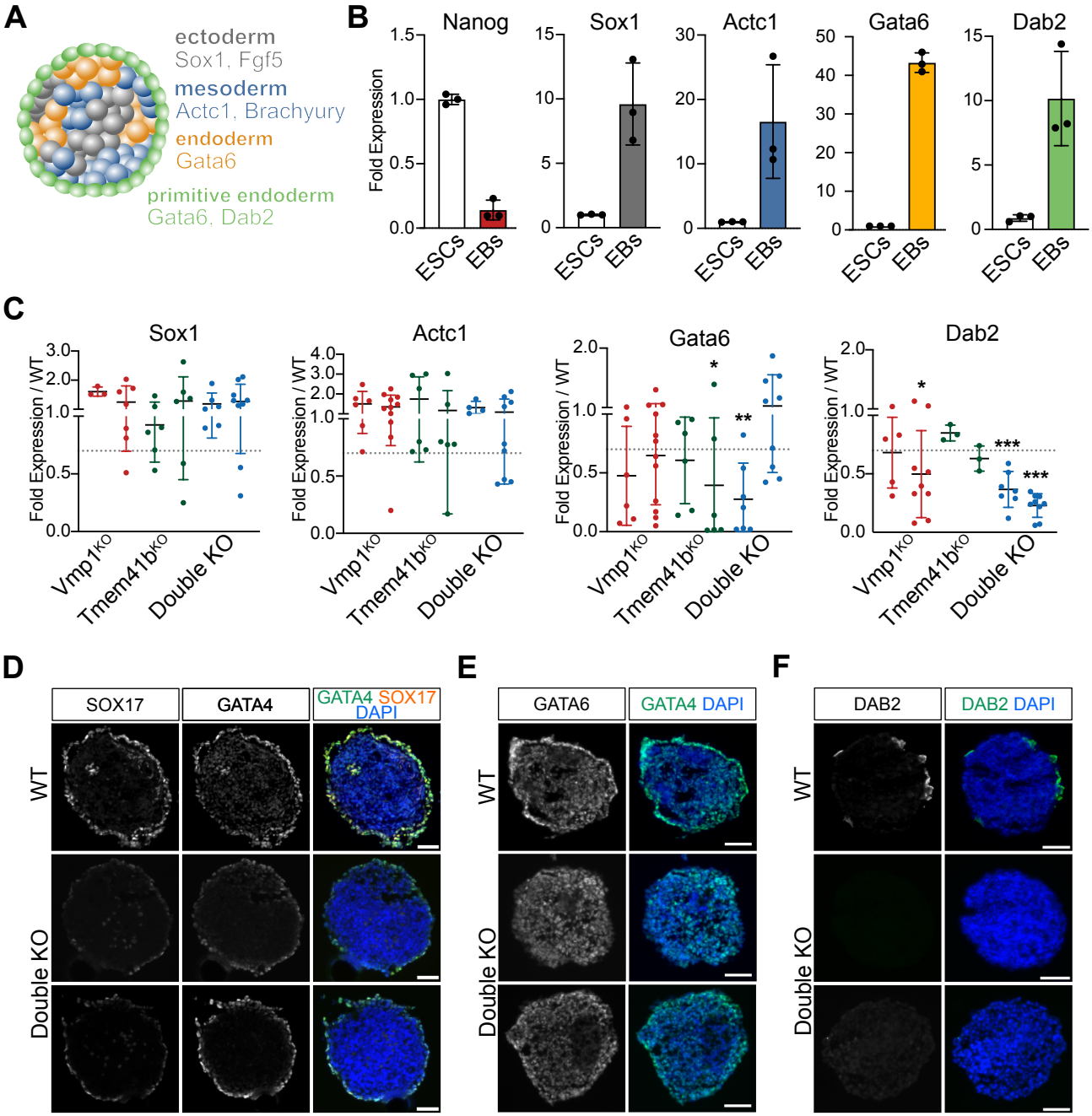
A
ectoderm
Sox1, Fgf5
mesoderm
Actc1, Brachyury
endoderm
Gata6
primitive endoderm
Gata6, Dab2
B
Nanog
Sox1
Actc1
Gata6
Dab2
Fold Expression
ESCs
EBs
C
Sox1
Actc1
Gata6
Dab2
Fold Expression / WT
Vmp1KO
Tmem41bKO
Double KO
D
SOX17
GATA4
GATA4 SOX17 DAPI
WT
Double KO
E
GATA6
GATA4 DAPI
F
DAB2
DAB2 DAPI

Figure 3

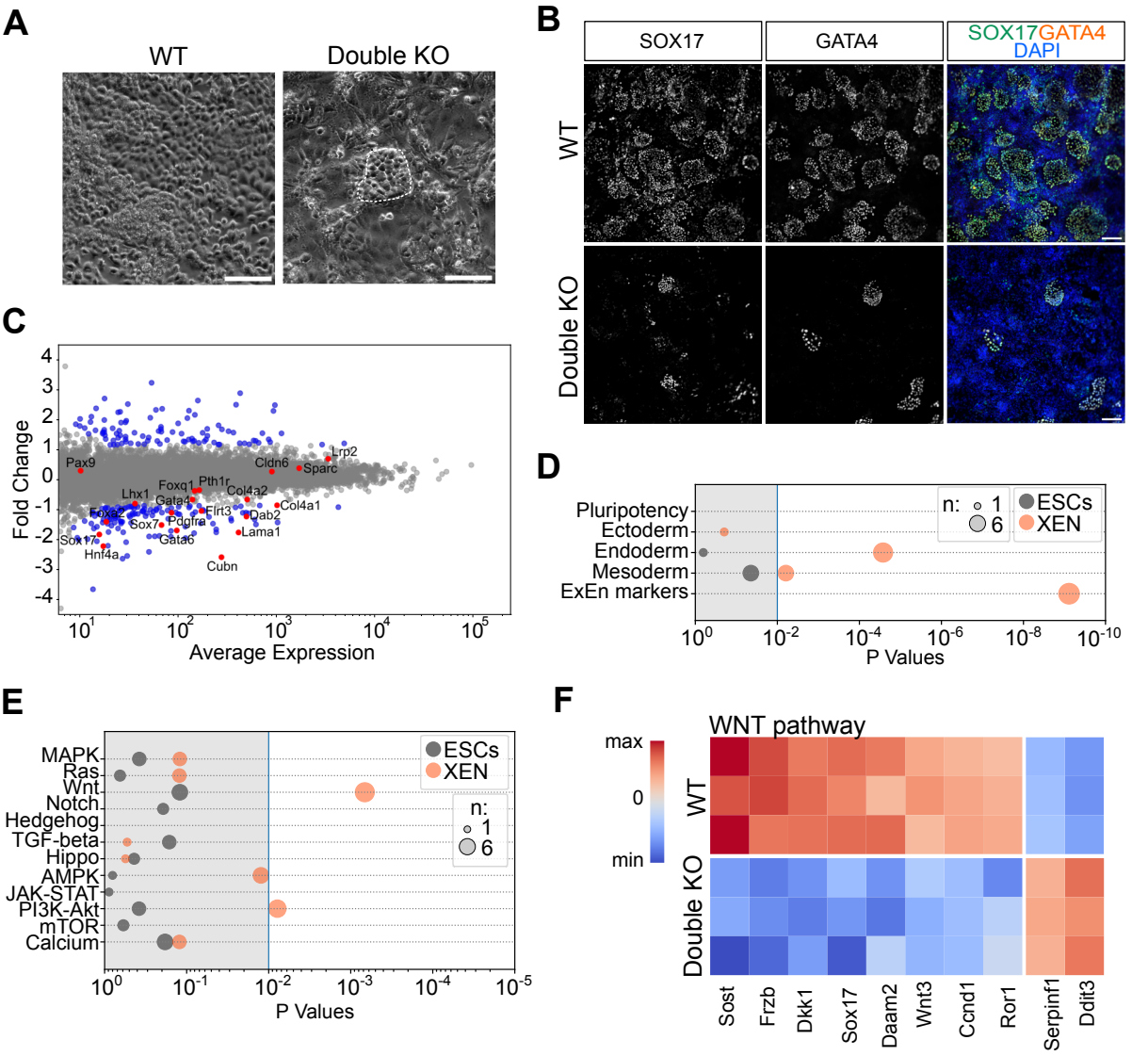
A
WT
Double KO
B
SOX17
GATA4
SOX17GATA4
DAPI
WT
Double KO
C
Fold Change
Average Expression
Pax9
Lrp2
Cldn6
Sparc
Foxq1
Pth1r
Col4a2
Lhx1
Gata4
Col4a1
Elf3
Dab2
Sox7
Pdgfra
Lama1
Sox17
Gata6
Hnf4a
Cubn
D
Pluripotency
Ectoderm
Endoderm
Mesoderm
ExEn markers
n:
1
6
ESCs
XEN
P Values
E
MAPK
Ras
Wnt
Notch
Hedgehog
TGF-beta
Hippo
AMPK
JAK-STAT
PI3K-Akt
mTOR
Calcium
ESCs
XEN
n:
1
6
P Values
F
WNT pathway
max
0
min
WT
Double KO
Sost
Frzb
Dkk1
Sox17
Daam2
Wnt3
Ccnd1
Ror1
Serpinf1
Ddit3

Figure 4

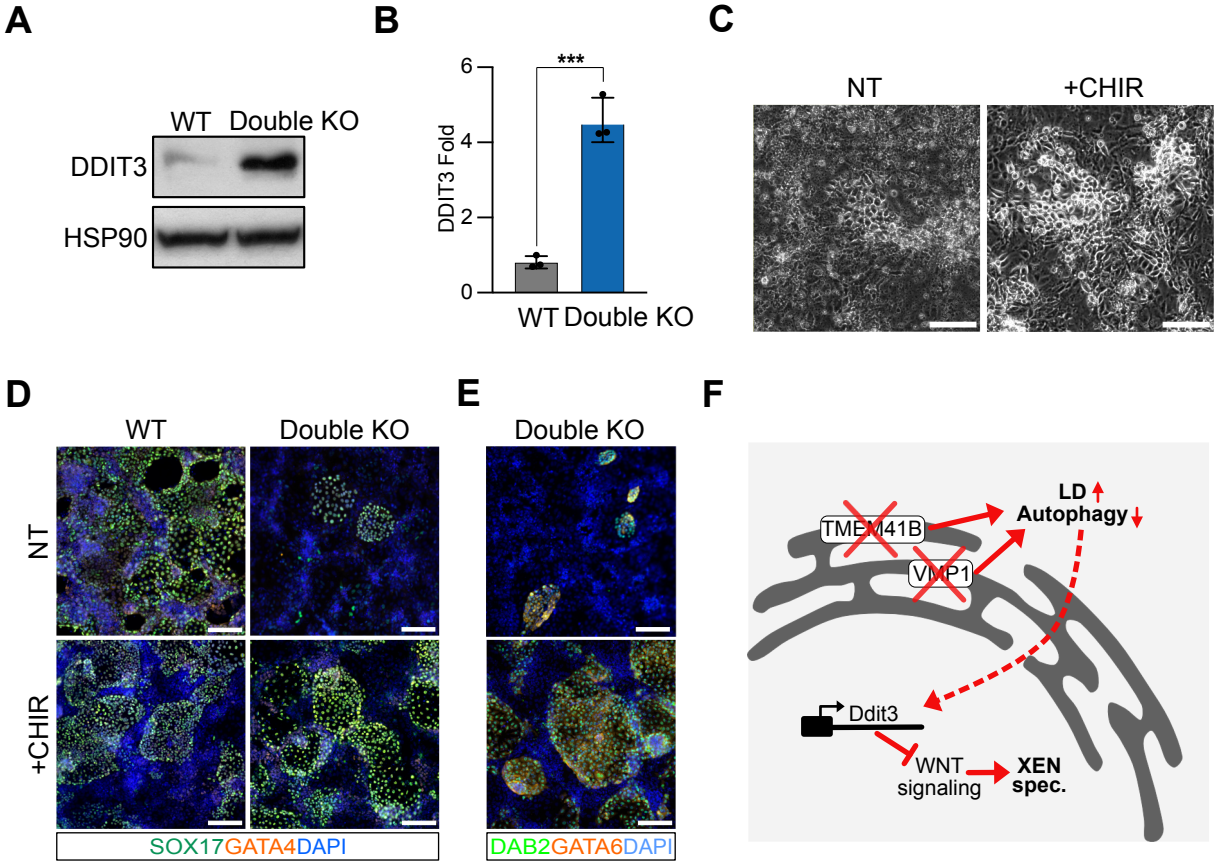
A
WT
Double KO
DDIT3
HSP90
B
***
DDIT3 Fold
6
4
2
0
WT
Double KO
C
NT
+CHIR
D
WT
Double KO
NT
+CHIR
SOX17GATA4DAPI
E
Double KO
DAB2GATA6DAPI
F
TMEM41B
VMP1
LD
Autophagy
Ddit3
WNT
signaling
XEN
spec.